Digital Beamforming Imaging Techniques for a Low Orbit Synthetic Aperture Radar Instruments

M. Younis[⊛], F. Stambouli[⊛], M. Zonno[⊛], S. Huber[⊛], G. Krieger[⊛], and K. Mouthaan[⊙]

[⊛] Microwaves and Radar Institute, German Aerospace Center (DLR), Oberpfaffenhofen, Germany
[⊙] National University of Singapore, Singapore

Abstract

The current trend in spaceborne imaging radar is towards compact SAR systems produced at a relatively low cost. At the same time, there is a tendency towards instruments equipped with digital beamforming (DBF) capabilities on transmit and receiver, which is attributed to available digital technology. These two trends are (seemingly) contradicting, since digital beamforming facilitates an improved imaging performance but generally does not allow for size, complexity, or cost reduction.
In this paper, we show that DBF may well be combined with compact SAR systems. It allows for the exploitation of elaborate imaging techniques customized to specific user requirements, which results in a simplified instrument hardware. The instrument and antenna design approach is for an L-band very low Earth orbit SAR system. Focus is put on the interrelation between the DBF imaging techniques and the instrument design. The calculated SAR performance is presented.

1 Mission Requirements

The primary particularities of the L-band SAR system is the low orbit height, h_{sat}, which varies from $225\,\mathrm{km}$ to $275\,\mathrm{km}$, further, the coverage is confined to $\pm 25^\circ$ latitude angles. This suggests a circular orbit (eccentricity, $e = 0$) of inclination $i \approx 25^\circ$ or $i \approx 115^\circ$ for a prograde (satellite moves in the direction of Earth's rotation) or retrograde orbit, respectively. The semimajor axis of the orbit is a consequence of the satellite's orbit height and varies accordingly. Noting the large variation of the access range with orbit height already indicates the complexity in defining the imaging parameters of a mapping mission, i.e. a mission that systematically images the Earth within the given latitude, for an uncontrolled (varying) orbit height.
The incident angle, η_i, should be in the range 20° to 45° which, given the orbit height, defines access range $135\,\mathrm{km}$ to $162\,\mathrm{km}$. The chirp bandwidth determines the value of the slant range resolution $\delta r_s = c_0/2B_w = 1.87\,\mathrm{m}$. The ground range resolution then varies with the incidence angle according to $\delta r_g = c_0/(2B_w \sin\eta_i)$. The variation of the ground range resolution may be mitigated either through image generation processing by a range-dependent multi-looking, or through the imaging mode: for example by reducing the transmit chirp bandwidth at far range. Aiming at a roughly square-shaped resolution cell suggests an azimuth resolution $\delta_{az} \approx 4\,\mathrm{m}$.

2 Digital Beamforming

The instrument design fully explore digital beamforming capabilities enabling sophisticated imaging techniques (SAR modes). The reader is assumed to be familiar with the basic (intrinsic) digital beamforming techniques known as Scan-On-ReceivE (SCORE) and Multiple Azimuth Channels (MACs) [1, 2, 3, 4, 5].
SCORE requires the beamwidth of the transmit antenna pattern to be wider than that of the receive pattern in elevation; whereas the transmit beamwidth (in azimuth) of MACs should be equal to that of an individual receive channel. Consequently, for a direct radiating planar antenna, the transmitting antenna area is smaller than the receiving one, both in azimuth and elevation. This may be used to the advantage of a simplified antenna front-end topology, where not all antenna elements are equipped with Transmit/Receiver Modules (TRM).

2.1 Sub-Pulse Imaging Technique

For fine azimuth resolution, the Pulse Repetition Frequency (PRF) must be sufficiently high to adequately sample the Doppler spectrum, which is inversely proportional to the antenna length. For linear quad-polarization operation, the instrument successively transmits H- and V-polarized electromagnetic waves; thus the minimum PRF value required for adequate azimuth sampling is doubled compared to single polarization.
The available time for receiving the radar echoes is $T_{pri} - \tau_p$, where $T_{pri} = 1/f_{prf}$ defines the Pulse Repetition Interval (PRI), and τ_p the transmit pulse duration. A sufficiently large PRI is necessary to accommodate the return echo. The width of the imaged swath is thus, among others, constrained by the instrument timing. These contradictory requirements on the PRF for achieving fine azimuth resolution and wide swath are well known [6]. It is also known that digital beamforming (DBF) allows relaxing, or even overcoming, these constraints [7].
One of DBF techniques utilizes sub-pulses [8]: here two (or more) pulses are transmitted within one pulse repeti-

tion interval illuminating different sub-swathes as shown in Fig. 1. The time difference between the transmission of the sub-pulses, ΔT_{sp}, is typically in the order of the pulse duration τ_p. Although the echo signals from the two sub-pulses arrive at distinct PRI intervals, the SAR instrument transmits successive pulses every PRI seconds, resulting in a nearly complete temporal overlap of the echo signals from sub-pulses transmitted at different PRI intervals. This is where DBF comes into use since it allows receiving and separating instantaneous echos arriving from different directions; in other words, two (or more) digital receive beams are generated, each one confined to one sub-swath, cf. Fig. 1. The added value of the sub-pulse technique is that it allows increasing the imaged swath width by "adding" sub-swathes without the need to reduce the PRF.

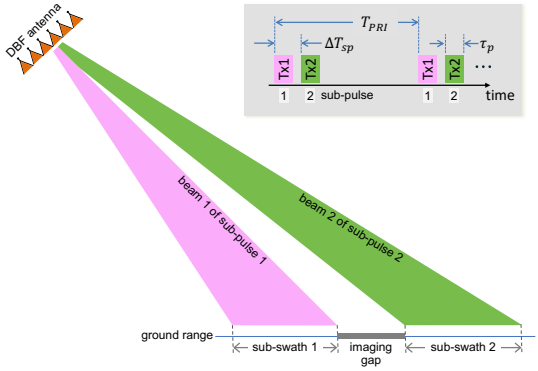


Figure 1: Visualization of the sub-pulse technique here for the case of two sub-pulses showing the antenna beams illuminating two different sub-swathes along with the corresponding sub-pulse timing.

For the SAR system considered here, two sub-pulses are utilized. Taking into account the quad-polarization, i.e., each sub-swath must be illuminated by alternating H- and V-polarization, gives two options for the sub-pulse sequence: transmit (Tx) sub-pulses of identical or orthogonal polarization. The decision affects two aspects: range ambiguity contamination and instrument front-end Tx topology, as explained in the following.

Cross-Pol. versus Co-Pol. Range Ambiguity

Without restriction of generality, it can be assumed that the first and second transmitted sub-pulses illuminate the first and second sub-swath, respectively.

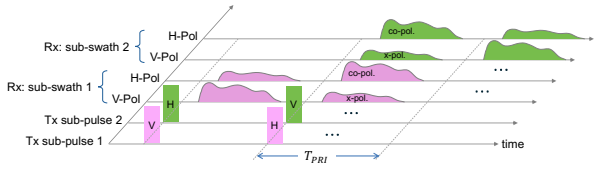


Figure 2: Favored sub-pulse polarization sequence. The color coding refers to Tx sub-pulse 1 and 2 as well as the corresponding return echoes from sub-swath 1 and 2, where each sub-pulse illuminates the same sub-swath.

The point to be addressed here is whether sub-pulses should transmit identical or orthogonal polarization. The latter is shown in Fig. 2 for the case of two transmit PRIs, which is sufficient for consideration. Since sub-pulse 1 and 2 illuminate two sub-swathes separated by one PRI in the timing diagram, respective return echoes of sub-pulse 2 are delayed by one PRI with respect to those of sub-pulse 1. As seen in the figure, the strong co-pol. return echoes from sub-swath 1 are contaminated by co-pol. range ambiguities arriving simultaneously from sub-swath 2. The same is true for the weak x-pol. return echoes. This sequence is favored because it prevents weak x-pol. returns to be contaminated by the strong co-pol. returns, which would require additional spatial range ambiguity suppression through the antenna pattern.

2.2 Instrument Tx Front-End Topology

Since the two transmitted sub-pulses are of orthogonal polarization, there is no need to equip every transmitting antenna element with both H and V polarizations. Instead each transmit antenna element is assigning to one polarization only, and the antenna elements of each polarization are assigned two sets of beamforming coefficients to illuminate sub-swaths 1 and 2. Since the two sub-pulses intended for different sub-swaths are of orthogonal polarization (H-pol and V-pol), they can be transmitted simultaneously, $\Delta T_{sp} = 0$, from different subsets of the antenna array.

As a result, each transmitting antenna element requires only one Tx amplifier and circulator, dedicated to its assigned polarization (either H-pol or V-pol). This avoids the need for all antenna elements to support dual-polarized transmission. The architecture enables full-pol operation while reducing the number of transmit amplifiers and circulators resulting in reduced front-end hardware complexity, lower power consumption, and cost. Here, the advantage is a reduction in both digital and RF hardware.

3 SAR Instrument Design

3.1 Repeat Cycle and Orbit Selection

The starting point for this instrument design is an orbit analysis to determine the required access range for a given repeat cycle in days. The circular orbits (eccentricity, $e = 0$) —described through Kepler's classical orbital elements— are inclined by $i \approx 25°$ or $i \approx 115°$ to cover areas between $\pm 25°$ latitude. Fig. 3 shows available orbit height and repeat cycle combinations; the numbers above and below each circle represent the number of orbits per repeat cycle and the ground track separation at the equator in kilometers; the latter represents the required imaged swath width to achieve complete coverage within the repeat cycle when imaging either on ascending or descending orbits.

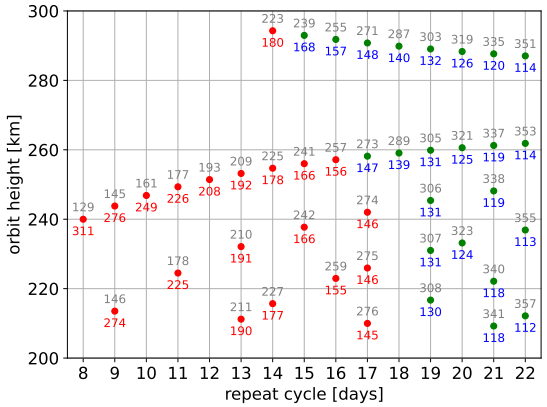


Figure 3: Orbits: available orbit height and repeat cycle combinations.

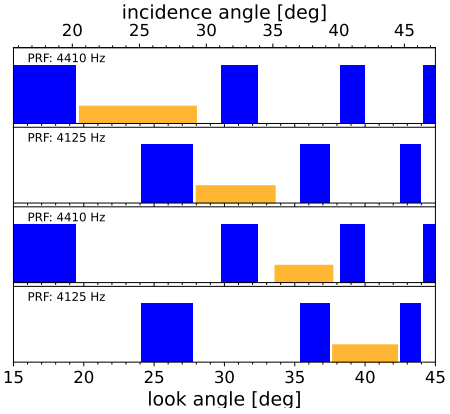


Figure 4: Sub-swath echo window position (orange boxes) and transmit events (blue boxes) versus incidence/look angle for $h_{sat} = 260\,\mathrm{km}$. Each row represents one sub-pulse at one PRF value.

The underlying assumption for determining the valid combinations is an orbit period, T_{orb}, calculated according to

$$T_{orb} = 2\pi\sqrt{\frac{(R_e + h_{sat})^3}{\mu}}, \tag{1}$$

where μ is the gravitational parameter $3.986 \times 10^5\,\mathrm{km}^3\,\mathrm{s}^{-2}$; h_{sat} the satellite orbit height in km; and R_e is the Earth's radius at the equator $6378.137\,\mathrm{km}$.

Ground track separations that result in an access range outside the $20°$ to $45°$ incidence angle limit are marked in red. From Fig. 3 the smallest repeat cycle is 17 days for an orbit height of $260\,\mathrm{km}$ and the ground track separation at the equator of $147\,\mathrm{km}$.

3.2 Acquisition Plan and Timing

The SAR of instrument A is considered a mapping mission for all latitudes between $\pm 25°$. This SAR system is capable of imaging two sub-swathes separated by a gap. To achieve contiguous imaging, the gap between the sub-swathes of one cycle is "filled" by the imaged sub-swathes of the second, and, in addition, the imaged sub-swathes of the two cycles must be contiguous as shown in Fig. 4. Within two cycles, the complete access range (corresponding to the ground track separation) is then imaged using either ascending or descending orbits. This results in a complete coverage at the equator, while for higher and lower latitudes there is even an overlap between the swathes.

As each orbit observes two separated sub-swaths, 1 and 2, this configuration inherently leaves an unobserved gap between the two illuminated regions. The strategy to fill the imaging gap is to use two consecutive repeat cycles, such that $\Delta D_g = 0$. Different sub-swathes must be imaged at the second cycle. In this case, the transmit beam for sub-swath 1 fully illuminates the gap region left by the previous cycle, since the sub-swath width exactly matches the gap, while sub-swath 2 extends the imaged swath. This method ensures seamless spatial coverage.

3.3 Antenna Size and Element Spacing

From a SAR operation and performance perspective, there is no upper limit to the Rx antenna height as SCORE is being used. The only complexity would arise if the pulse extension loss (PEL) increases, which would require dispersive beamforming [9, 1]. On the other hand, practical constraints such as the launcher, antenna folding mechanisms, orbit keeping, etc. suggest not exceeding a specific height.

The Tx antenna height depends on the width and angular position of the illuminated sub-swath. Fig. 5 shows the antenna height versus the illuminated swath. A large Tx antenna height has an intrinsic beamwidth that is too small, thus requiring phase spoiling beamforming to widen the beam. This is not necessarily a disadvantage, since a higher antenna means more antenna elements and more Tx power due to the larger number of TRMs. If the antenna height is too small, areas outside the imaged swath are illuminated, i.e., power is "wasted", further the range ambiguity performance degrades. Here, sub-swath 2 of cycle 2 is the most restrictive case which with Fig. 5 suggests an antenna height in the order of $3\,\mathrm{m}$.

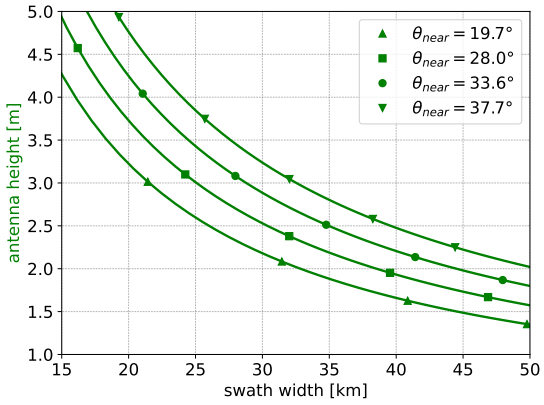


Figure 5: Antenna height versus swath width with the sub-swath near range look angle as a parameter.

The antenna length is determined by the PRF, the processed Doppler bandwidth, and the number of azimuth channels. Furthermore, an azimuth sampling uniformity between $90\,\%$ to $110\,\%$ is desirable, or otherwise the SNR scaling will result in a worsening of the NESZ. Using the timing and orbit parameters to calculate the uniform antenna length results in $7\,\mathrm{m}$ and $7.5\,\mathrm{m}$ for the PRF of cycles 1 and 2, respectively. The antenna can be shortened but the processed Doppler bandwidth must also reduced for an acceptable AASR level; however, then Tx power is "wasted" because the illuminated Doppler bandwidth is larger than what is required.

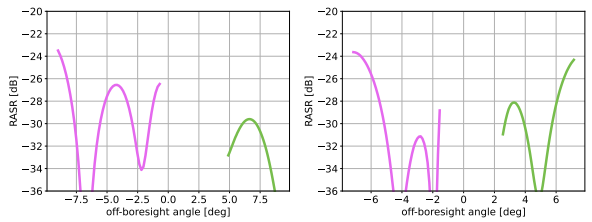
The antenna element elevation spacing depends on the maximum scan angle, which depends on the access range. If satellite role manouvers are allowed between cycle 1 and 2 the required access range corresponds to the difference between the far range look angle of sub-swath 2 and the near range look angle of sub-swath 1 which results in a 0.851λ spacing.

4 SAR Instrument Performance

The performance is reported in terms of the range and azimuth ambiguity-to-signal ratios as well as the noise-equivalent sigma-zero.

4.1 Range-Ambiguity-to-Signal Ratio

The range-ambiguity-to-signal ratio (RASR) of repeat cycles 1 and 2 shown in Fig. 6 are below $-23\,\mathrm{dB}$. The highest ambiguity levels appear at the near range of sub-swath 1 and are caused by the sub-pulse transmit pattern coupling, which cannot be attenuated through the receiver pattern



(a) repeat cycle 1 (b) repeat cycle 2

Figure 6: Range ambiguity performance versus antenna off-boresight angle for sub-swath 1 and 2.

To explain this effect, Fig. 7 shows the transmit, receive, and 2-way elevation patterns for three different SCORE beams for sub-swath 1 of cycle 1. The two Tx patterns are activated simultaneously, either through DBF on transmit or by using different panels of the antenna, for transmitting sub-pulse 1 and 2, respectively. The beamwidth of the transmit patterns should match the respective angular sub-swath width, while, at the same time the main lobe overlap and side-lobe level in the direction of the "other" sub-swath should be minimized. The reason is that in the case of the sub-pulse technique, the transmit pattern overlap inherently results in range ambiguities, which cannot be attenuated through the receiver pattern. This is why a transmit amplitude taper is applied here.

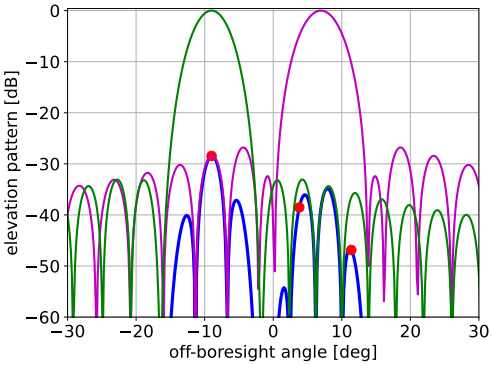


Figure 7: Transmit (magenta), receive (green), and two-way (blue) radiation patterns at the near range of sub-swath 1 with the position of the range ambiguities shown by the red circles.

Note that the width of the Rx SCORE patterns is comparable to that of the transmit pattern, which is a result of both Tx and Rx antennas having similar heights. The consequence of this is that the number of SCORE beams can be reduced to 3 to 9 per sub-swath without significantly impacting the ambiguity performance or the NESZ. This simplifies the digital SCORE implementation and the required number of beamforming coefficients.

4.2 Azimuth-Ambiguity-to-Signal Ratio

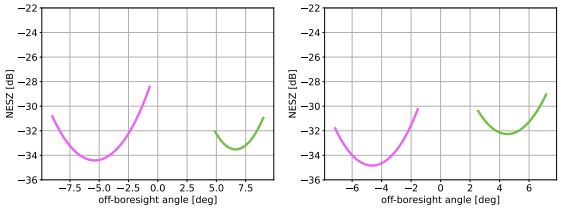
The Azimuth Ambiguity-to-Signal Ratio (AASR) is a key metric for evaluating azimuth performance. Both repeat cycles achieve AASR $< -23\,\mathrm{dB}$. Repeat cycle 1 achieves a significantly lower AASR of $-27.1\,\mathrm{dB}$, providing much better azimuth ambiguity performance. Repeat cycle 2 yields an AASR of $-23.1\,\mathrm{dB}$, still within the requirements. The resolution values for cycle 1 and 2 are $3.38\,\mathrm{m}$ and $3.6\,\mathrm{m}$, respectively.

The processed Doppler bandwidth $< 2.3\,\mathrm{kHz}$ which is much lower than the PRF $> 4.1\,\mathrm{kHz}$ indicates a high oversampling in azimuth. This may be leveraged by applying the Azimuth Phase Coding (APC) technique [10]. This introduces a cyclic shift in the azimuth pattern of the range ambiguity, resulting in a further suppression of the range ambiguity. This combination of the sub-pulse technique with azimuth phase coding is patented [11, 12]. Its APC gain, which is the added attenuation of the range ambiguities is in the order of $3.5\,\mathrm{dB}$ and $3.1\,\mathrm{dB}$ for cycle 1 and 2, respectively.

4.3 Noise Equivalent Sigma Zero

The parameter determining the noise performance is the Noise Equivalent Sigma Zero (NESZ) which represents the backscatter value resulting in an SNR of $0\,\mathrm{dB}$. Fig. 8

shows the NESZ for an average transmit power $P_{av} = 273\,\mathrm{W}$, a noise figure of $3.5\,\mathrm{dB}$ and $1\,\mathrm{dB}$ antenna losses. The good performance (low NESZ values) for a reasonable average transmit power result from the efficient illumination, since only two sub-swathes are illuminated using a high antenna gain; the low orbit height (slant range to the enters the NESZ with R^3); relatively long pulse duty cycle of $13\,\%$.



(a) repeat cycle 1 (b) repeat cycle 2

Figure 8: Noise equivalent sigma zero (NESZ) versus off-boresight angle for sub-swath 1 and 2.

Factors degrading the noise performance are the strong amplitude taper on transmit which results SNR degradation from $3.8\,\mathrm{dB}$ to $6.1\,\mathrm{dB}$. Although the transmit amplitude taper is implemented digitally, the transmit amplitude taper results in huge losses, because the actual amount of power is reduced. This is the cost of operating the system in the sub-pulse mode, where the transmit taper is the only way to suppress the mutual range ambiguities. The amplitude taper on-receive only results in a small SNR degradation of less than $1\,\mathrm{dB}$, because it is implemented in the digital domain.

5 Conclusion

A instrument and antenna design for a compact SAR system is presented which fully utilizes digital beamforming capabilities. It is shown, that DBF can be used to the advantage of a simplified instrument design, since it allows for the implementation of advanced imaging techniques. Further, DBF facilitates achieving good imaging performance.

Acknowledgment

This research is supported by the Office for Space Technology & Industry (OSTin) of the Economic Development Board, Singapore.

References

[1] M. Younis, F. Q. de Almeida, M. Villano, S. Huber, G. Krieger, and A. Moreira, "Digital beamforming for spaceborne reflector-based synthetic aperture radar. Part 1: Basic imaging modes," *IEEE Geoscience and Remote Sensing Magazine*, vol. 9, no. 3, Sept. 2021.

[2] ——, "Digital beamforming for spaceborne reflector-based synthetic aperture radar. Part 2: Ultra-Wide swath imaging mode," *IEEE Geoscience and Remote Sensing Magazine*, vol. 10, no. 4, Dec. 2022.

[3] N. Gebert, G. Krieger, and A. Moreira, "Digital beamforming on receive: Techniques and optimization strategies for high-resolution wide-swath SAR imaging," *IEEE Transactions on Aerospace and Electronic Systems*, vol. 45, pp. 564–592, 2009.

[4] G. Krieger, N. Gebert, and A. Moreira, "Unambiguous SAR signal reconstruction from non-uniform displaced phase centre sampling," *IEEE Geoscience and Remote Sensing Letters*, vol. 1, no. 4, pp. 260–264, Oct. 2004.

[5] M. Süß, B. Grafmüller, and R. Zahn, "A novel high resolution, wide swath SAR," in *Proceedings Int. Geoscience and Remote Sensing Symposium IGARSS'01*, vol. 3, Sydney, Australia, July 2001, pp. 1013–1015.

[6] A. Freeman, W. Johnson, B. Huneycutt, R. Jordan, S. Hensley, P. Siqueira, and J.Curlander, "The 'Myth' of the minimum SAR antenna area constraint," *IEEE Transactions on Geoscience and Remote Sensing*, vol. 38, no. 1, pp. 320–324, Jan. 2000.

[7] M. Younis, C. Fischer, and W. Wiesbeck, "Digital beamforming in SAR systems," *IEEE Transactions on Geoscience and Remote Sensing*, vol. 41, no. 7, pp. 1735–1739, July 2003.

[8] M. Younis, G. Krieger, and A. Moreira, "MIMO SAR techniques and trades," in *Proceedings of the European Radar Conference (EuRAD)*, Nuremberg, Germany, Oct. 2013, pp. 141–144.

[9] M. Younis, T. Rommel, F. Bordoni, G. Krieger, and A. Moreira, "On the pulse extension loss in digital beamforming SAR," *IEEE Geoscience and Remote Sensing Letters*, vol. 12, no. 7, pp. 1436–1440, July 2015.

[10] J. Dall and A. Kusk, "Azimuth phase coding for range ambiguity suppression in SAR," in *Proc. Int. Geoscience and Remote Sensing Symposium (IGARSS'2004)*, vol. 3, Anchorage, AK, USA, July 2004.

[11] M. Younis, F. Bordoni, G. Krieger, P. López-Dekker, and F. D. Zan, "Synthetik-apertur-radarverfahren und synthetik-apertur-radarsystem," German Patent Patent DE 10 2013 221 756, Oct., 2014.

[12] ——, "Synthetik-Apertur-Radarverfahren und Synthetik-Apertur-Radarsystem," European Patent Patent EP 3 060 939 B1, Nov., 2018.